(Received 1 February 2024, Accepted 9 July 2024, Scheduled 24 July 2024)

Optimal Service Area Partitioning for Wireless Communication Systems and a Multibeam Antenna with Contoured Beams for the Equipotential Coverage of This Area

Alexander V. Shishlov[1,2], Yury V. Krivosheev[1,2,3,*], Vladimir V. Denisenko[1,3], and Boris A. Levitan[1,3]

[1]JSC "Radiofizika", Moscow 125363, Russia
[2]Moscow Institute of Physics and Technology, Dolgoprudny, Moscow 141701, Russia
[3]Moscow Institute of Aviation, Moscow 125993, Russia

ABSTRACT: In a number of wireless communication systems with multibeam antennas, the distance from the antenna to subscribers in different parts of the service area varies significantly. Such systems include high-altitude platform station communication systems, communication systems based on low Earth orbit and medium Earth orbit satellites, and several others. If such a system uses an antenna with identical beams, the throughputs of communication lines in different cells can differ by more than an order of magnitude due to the variation in distance. To equalize throughputs across all cells within the service area, an antenna with different beams can be employed. The gain of these beams should be proportional to the squared slant ranges to the centers of the served cells. The gain of a beam can be modified by altering its size and shape. This paper proposes a method for service area partitioning in communication systems that accounts for the slant range to subscribers. It determines the shapes and profiles of the ideal contoured beams and presents optimized contoured beams for a real antenna.

1. INTRODUCTION

Various wireless communication systems with multibeam antennas (MBAs) have been developed in recent decades. Along with well-established communication systems such as satellite and cellular communication systems, several promising new systems have emerged. For instance, a significant number of articles have been published on high-altitude platform station (HAPS) communication systems [1–10]. HAPS is expected to utilize stratospheric dirigibles flying at altitudes of 18–25 km. The International Telecommunication Union (ITU) has issued recommendations that define the requirements for HAPS to provide different services in the S-, Ka-, and V-bands [6–8].

The key part of an HAPS is an MBA with the field of view being the cone with vertex angle 100°–150°. The beams of the MBA cover the circular service area (SA) on the Earth's surface with a diameter of 60–160 km.

In [9] and [10], S- and Ka-band MBAs based on active phased arrays with digital beamforming have been designed and tested. As follows from published works, MBAs having 200–400 narrow beams are necessary for SA coverage. Each beam serves its own cell in the SA.

The publications have highlighted that the distance from the HAPS to the subscribers within the SA varies by about four times. Consequently, the throughputs of communication lines in different cells can differ by more than an order of magnitude when identical beams are used. This disparity results in inequality for users located at different points within the SA.

The feasibility of forming beams with gain proportional to the squared distance from a transmitter to a receiver to equalize the throughputs of communication channels has been noted, for example, in [10].

A similar issue arises in communication systems based on low Earth orbit and medium Earth orbit (LEO/MEO) satellites. A concept for equalizing throughputs of communication channels in such systems is discussed in [11]. It is recommended to use a satellite MBA with beam gain proportional to the squared slant ranges to the centers of the served cells. However, [11] and other papers and books on communication systems with MBAs, such as Iridium and Globalstar [12–15], do not delve into methods for equalizing throughputs of communication lines, particularly by adjusting the shapes and sizes of the cells.

Equalizing the illumination of an SA can be achieved by forming contoured (shaped) radiation patterns. Studies [16–19] have shown that increasing antenna aperture dimensions and optimizing the contoured radiation pattern can enhance SA illumination at the edge of coverage (EOC) by 2–5 dB compared to pencil beams. This improvement is even greater in cases of complex SA shapes. Additionally, the sidelobe envelope level of the shaped radiation pattern can be significantly reduced to −30 dB or lower [20], facilitating high levels of beam decoupling and consequently increasing the information capacity of communication systems.

* Corresponding author: Yury V. Krivosheev (krivosheev-yury@yandex.ru).

It is important to note that MBAs with contoured beams can also be applied in other communication systems, including those utilizing base stations or repeaters, such as communication systems via stratospheric airplanes [21] and cellular systems (3G, 4G [22–24], 5G [25]).

The purpose of this work is to design an optimal method for partitioning an SA into cells, considering the slant range from a station to a subscriber, based on the MBA concept with ideal (optimal) contoured radiation patterns. Additionally, it aims to determine the profiles of the perfectly shaped beams in each cell. The synthesis of a real MBA is also addressed, with examples of antenna systems representing a multi-panel phased array with shaped beams, as well as an MBA comprising a conglomerate of aperture antennas with optimal beamwidths for covering SA cells in stratospheric communication systems [26].

2. CIRCULAR SA

Let us first consider the problem of achieving equipotential SA coverage (equal power flow) on a flat surface with a single-beam antenna on a platform suspended at height h (Fig. 1). The SA is a circle with a radius r_{SA}, with the circle center O coinciding with the projection of the antenna center on the serviced plane.

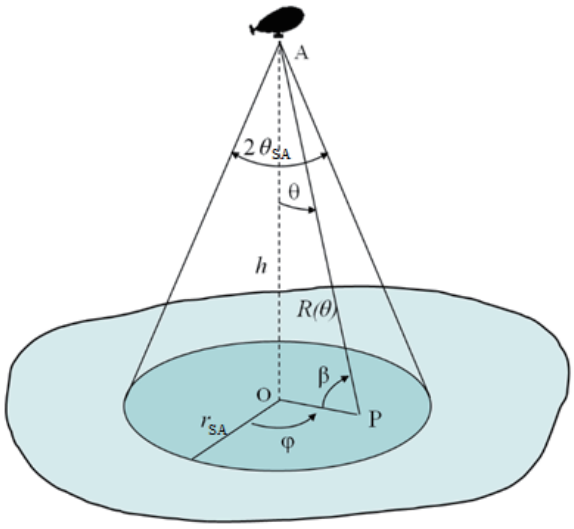

FIGURE 1. Circular SA and the antenna above it, located on a dirigible, balloon, or other platform.

The antenna field is a nonuniform spherical wave; therefore, for the equipotential illumination (coverage) of the SA, the following condition must be met:

$$|F(\theta,\varphi)|/R(\theta) = const, \tag{1}$$

where $F(\theta,\varphi)$ is the antenna radiation pattern, and $R(\theta)$ is a slant range from the antenna to a serviced point P.

The slant range depends on the angular coordinate θ only (Fig. 1) and does not depend on φ. In the case of a flat surface, it is defined by the following proportion:

$$R(\theta) = h \cdot \sec\theta. \tag{2}$$

Outside the SA where there are no subscribers, there must be no antenna radiation; therefore, such a perfectly shaped radiation pattern normalized to the value in the axial direction is as follows:

$$|F_{perf}(\theta)|^2 = \begin{cases} \sec^2\theta \equiv csc^2\beta, & \theta \le \theta_{SA}, \\ 0, & \theta > \theta_{SA}, \end{cases} \tag{3}$$

where $2\theta_{\text{SA}}$ is the angular size of the SA (Fig. 1).

Let us define the angular dependence of the perfect gain profile through the directive gain corresponding to the perfect contoured radiation pattern assuming no losses in the antenna:

$$G_{perf}(\theta,\varphi) = \frac{4\pi\,|F_{perf}(\theta,\varphi)|^2}{\int_0^{2\pi}\int_0^{\theta_1} |F_{perf}(\theta',\varphi')|^2 \sin\theta' d\theta' d\varphi'} \tag{4}$$

From (4), taking (3) into account, we obtain the following:

$$G_{perf}(\theta,\theta_{SA}) = \begin{cases} \dfrac{2\sec^2\theta}{\sec\theta_{SA}-1} = G_0\cdot\sec^2\theta, & \theta \le \theta_{SA} \\ 0, & \theta > \theta_{SA} \end{cases} \tag{5}$$

Angular dependencies of the gain (5) and the contoured radiation pattern (3) coincide up to a normalizing factor defined by the SA angular size.

The perfect gain values (5) are defined by the problem geometry only and do not depend on the antenna parameters.

In Fig. 2, the plots for $G_{perf}(\theta,\theta_{\text{SA}})$ are shown for several θ_{SA} values.

With $\theta_{\text{SA}} \to 90°$, the distance to the SA border increases infinitely; therefore, $G_{perf}(\theta_{\text{SA}},\theta_{\text{SA}}) \to \infty$, and in the direction $\theta = 0°$ (i.e., nadir), the gain approaches zero $G_{perf}(0,\theta_{\text{SA}}) \to 0$.

The perfect contoured beam under consideration has infinitely steep slopes at the SA borders and zero values outside the SA, which is impossible to achieve in practice. Real antennas with finite dimensions and shaped radiation patterns exhibit transition zones of finite width at the SA border, lower gain within the SA, and sidelobes outside it.

From the proportion (5) and Fig. 2, it is evident that for large values of the SA angular size $2\theta_{\text{SA}}$, a single-beam antenna with a contoured radiation pattern designed for wide-angle area service has low gain. Such antennas are unsuitable for high-throughput communication systems.

In the case of a narrow service sector, when the θ_{SA} angle is small, the gain (5) comes down to a known expression for the gain of an antenna with a uniform perfect contoured radiation pattern [27]:

$$G_{perf} = \frac{1}{\sin^2(\theta_{SA}/2)} = \frac{4\pi}{\Omega} \tag{6}$$

where Ω is the spatial angle defining the angular size of the SA.

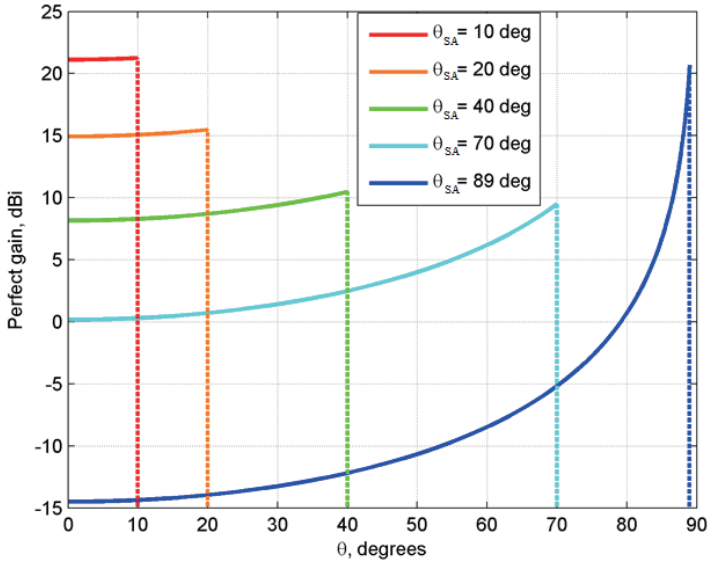

FIGURE 2. Angular dependencies of the perfect gain for a circular SA with different angular sizes.

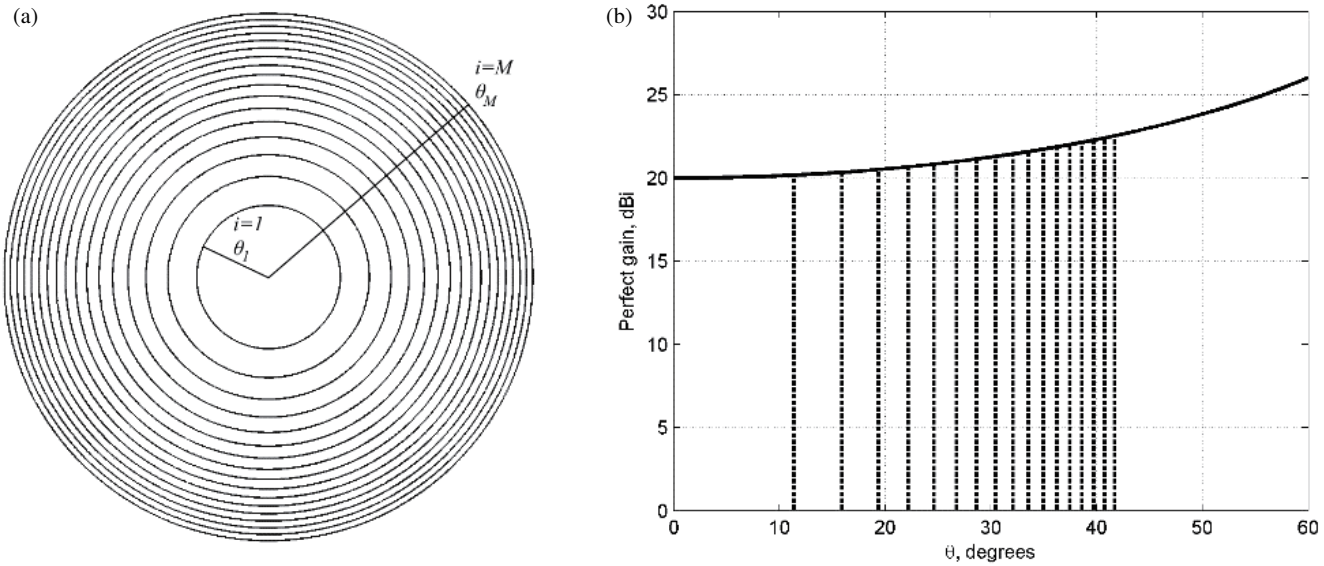

FIGURE 3. Circular SA with partitioning into ring-shaped cells: (a) cell geometry for $G_0 = 20$ dBi, $\theta_1 \approx 11.4°$, $\theta_{17} \approx 41.7°$ ($M = 17$ cells shown); (b) angular dependence of the perfect gain within the SA (the vertical dashed lines are cell borders).

3. SA WITH CIRCULAR RINGS

To increase the gain in the SA, it is partitioned into cells. Each cell is serviced with a separate beam.

Let us consider partitioning the circular SA into a system of concentrical rings (Fig. 3).

The first circular line ($i = 1$) is the border of the first cell. We specify its angular size $2\theta_1$ based on the condition that it is covered by a perfect contoured beam (3) with a specified value of the perfect nadir gain G_0. As follows from (5), the angular size of the cell and the nadir gain are related to each other in the following way:

$$\theta_1 = \arccos(G_0/(G_0 + 2)) \tag{7}$$

The next cells have the shapes of coaxial rings. Their total number M depends on the SA angular size. For the equipotential SA coverage according to condition (1), we extrapolate function (5) defining the perfect gain in the first cell to all other SA cells, as follows:

$$G_{perf}(\theta, \theta_1) = \begin{cases} \dfrac{2\sec^2\theta}{\sec\theta_1 - 1} = G_0 \cdot \sec^2\theta, & \theta \le \theta_M, \\ 0, & \theta > \theta_M. \end{cases} \tag{8}$$

In (8), the connection between θ_1 and G_0 defined in (7) has been taken into account.

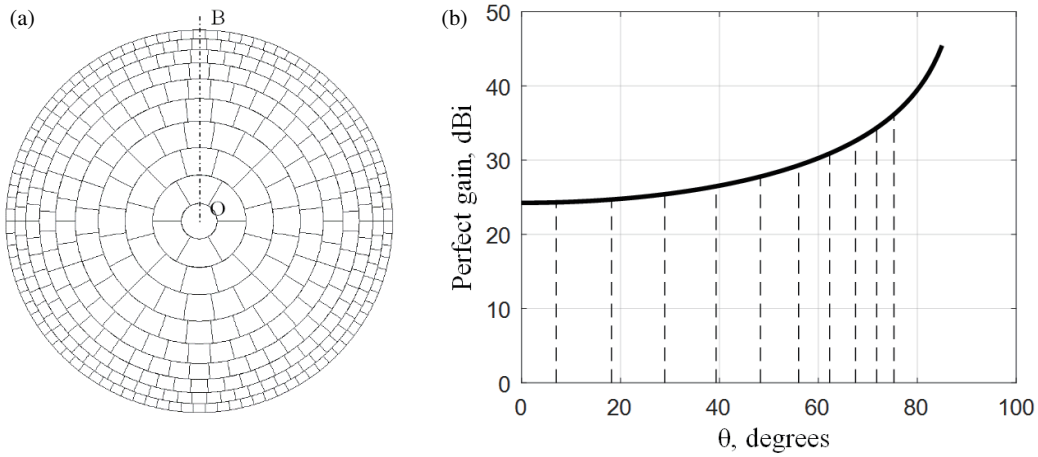

FIGURE 4. Circular SA partitioned into cells with a radial-and-ring grid: (a) cell geometry for $G_0 \approx 24.3$ dBi, $\theta_1 = 7°$, $M = 10$ rings, $\theta_{10} \approx 75.3°$, $\Delta\theta_{10} \approx 3.5°$; (b) angular dependence of the perfect gain in the SA (the vertical dashed lines are cell borders (12)).

The ring sizes are derived from the condition that perfect gain values within all rings must satisfy the following normalization:

$$\int_0^{2\pi}\int_{\theta_i}^{\theta_{i+1}} G_{perf}(\theta',\varphi')\sin\theta' d\theta' d\varphi' = 4\pi \qquad (9)$$

Substituting (8) into (9) and integrating them, we obtain the following recurrent relation for determining the radii of the rings:

$$\sec\theta_{i+1} = \sec\theta_i + \sec\theta_1 - 1 = \sec\theta_i + 2/G_0 \qquad (10)$$

where $i = 1, 2, \ldots M-1$.

The cell number M is defined from the condition that the outer ring has an angular radius θ_M not less than the specified SA radius θ_{SA}.

In Fig. 3, an example of SA partitioning based on the proportion (10) is shown. Perfect nadir gain is specified to be $G_0 = 20$ dBi, and according to (7), the central circle has a radius $\theta_1 \approx 11.4°$. The ring width decreases rapidly with the growth of i. Thus, the 17th ring with an outer radius $\theta_{17} \approx 41.7°$ has a width $\Delta\theta_{17}$ less than 1°. For the coverage of such a narrow ring-shaped cell, an antenna with a size of more than 50 wavelengths and an axisymmetric funnel-shaped radiation pattern is required. For instance, it can be a linear or cylindrical array, whose axis is directed toward the nadir, and the amplitude-phase distribution is synthesized to form the required profile for every contoured beam within the ring-shaped cell formed by the cones $[\theta_i, \theta_{i+1}]$.

4. SA WITH CELLS FORMED WITH A RADIAL-AND-RING GRID

For creating cells with higher gain than in the SA with ring-shaped cells (8) and (10), we partition the rings shown in Fig. 3 (except the center circle) into n_i parts with radial lines $\varphi_i = const$ forming cells with the shape of identical sectors with angular sizes $\Delta\varphi_i = 2\pi/n_i$.

Similar to the ring-shaped cells, we define the perfect gain in all the sector cells by the proportion (8). For that, the following normalization condition must be satisfied:

$$\int_0^{2\pi/n_{i+1}}\int_{\theta_i}^{\theta_{i+1}} G_{perf}(\theta',\varphi')\sin\theta' d\theta' d\varphi' = 4\pi \qquad (11)$$

Substituting (8) into (11) and integrating them, we obtain the following recurrent relation for determining the radii of the rings:

$$\sec\theta_{i+1} = \sec\theta_i + n_{i+1}\cdot(\sec\theta_1 - 1) = \sec\theta_i + 2n_{i+1}/G_0 \qquad (12)$$

For efficient illumination of the cells, we choose their transversal median size in each i-th ring equal to the radial size of that ring. Then for $i \geq 1$, we obtain the following:

$$n_{i+1} = [2\pi\cdot 0.5\cdot(\sin\theta_i + \sin\theta_{i+1})/(\theta_{i+1} - \theta_i)] \qquad (13)$$

where $[A]$ is the integer part of the number A, $[A] \leq A$.

Solving together the recurrent system of transcendent Equations (12) and (13) for the variables n_{i+1} and θ_{i+1}, where $i = 1, 2, \ldots M-1$, we obtain the numbers of sectors in rings and the angular coordinates of these rings' borders.

Figure 4(a) shows the cells obtained with the partitioning algorithm considered above for the case when the nadir gain amounts to $G_0 \approx 24.3$ dBi, $\theta_1 = 7°$. The opening angle of the SA amounts to $\theta_{SA} = \theta_{10} \approx 75.3°$. The SA is partitioned into $M = 10$ rings, with the number of cells in rings being $n_1 = 1$, $n_2 = 6$, and further up to $n_{10} = 98$, 391 cells in total. The angular dependence of the gain (8) and the borders of the rings are shown in Fig. 4(b).

A comparison of Figs. 3 and 4 reveals that with SA partitioning using a radial-and-ring grid, the cells are significantly wider than with the ring SA partition. Specifically, the angular size of the cells in the outer SA ring is about 3.5°. For servicing such cells, an antenna with an aperture size less than 17 wavelengths is sufficient.

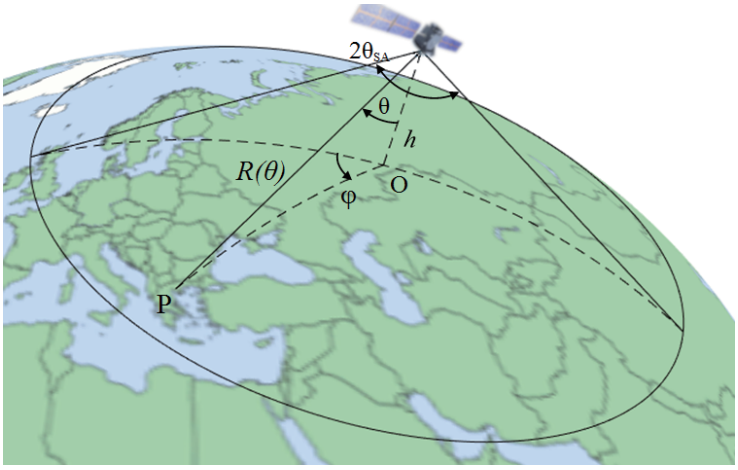

FIGURE 5. Circular SA on the Earth's surface in the case of the satellite being the antenna carrier.

The number of cells obtained by partitioning the SA into perfect contoured beams with specified nadir gain is defined by the following formula:

$$N = \frac{2G_0}{\sec\theta_{SA} - 1}. \tag{14}$$

Formula (14) holds true for both ring and radial-and-ring SA cell partitions

5. SA ON A SPHERICAL SURFACE

In a variety of problems, the serviced surface cannot be considered flat. For instance, if the antenna is satellite-borne (Fig. 5), its height above the surface h can be close to the Earth's radius, and to find the slant range to the observation point P, the following relation should be used [11]:

$$R(\theta, h, R_E) = \cos\theta\left(h + R_E - \sqrt{R_E^2 - \tan^2\theta\cdot(h^2 + 2hR_E)}\right) \tag{15}$$

where h is the satellite altitude, and R_E is the Earth's radius. The function (15) increases more rapidly with the increase in θ than (2) and achieves the maximum when the observation point is on the horizon. With $h \to 0$, formula (15) comes down to formula (2).

The expression for the perfect contoured radiation pattern providing equipotential illumination of the circular SA on the spherical surface is obtained from the condition (1) with the substitution of (15) into it:

$$|F_{perf}(\theta, R_E/h)|^2 = \begin{cases} \cos^2\theta\left(1+\frac{R_E}{h} - \sqrt{\left(\frac{R_E}{h}\right)^2 - \tan^2\theta\left(1+\frac{2R_E}{h}\right)}\right)^2, & \theta \le \theta_{SA} \\ 0, & \theta > \theta_{SA} \end{cases} \tag{16}$$

The perfect gain is obtained by substituting the contoured radiation pattern from Equation (16) into Equation (4) and then integrating them [11].

The spherical shape of the Earth notably influences the results of SA partitioning into cells and the profile of the perfect gain for altitudes h of the antenna suspension above the surface of the same order as the Earth's radius R_E. For small heights $h/R_E \ll 1$, the correlations derived before for the flat surface can be used.

For example, in the case of satellite placement on the Earth's orbit $h = 1,300$ km high ($R_E = 6,370$ km), the perfect gain in accordance with (16) exceeds the gain (8) by 0.5 dB for $\theta > 36°$ (the angle yielding the Earth's horizon direction at this altitude is $\theta_E = 56°$). For suspension of the antenna on a stratospheric dirigible on $h = 22$ km, the same gain difference for flat and spherical serviced surfaces is achieved for $\theta > 80°$, θ_E being 85°.

SA partitioning into ring cells on the spherical surface can be done with the algorithms described in the previous sections. However, (16) should be substituted into (9) (instead of (8)). SA partitioning into cells with a radial-and-ring grid on the spherical surface can be done by substituting (16) into (11).

6. MBA SYSTEM WITH SHAPED BEAMS

As an example of the coverage of an SA partitioned into cells with a radial-and-ring grid (Fig. 4), we consider a system of shaped beams formed with an S-band stratosphere communication antenna system based on a dirigible at an altitude of 22 km that was proposed earlier [10]. The antenna system is composed of seven identical phased arrays with circular apertures (Fig. 6). The central phased array is aimed at the nadir, and the inclination angle of the lateral phased arrays to the nadir amounts to 60°.

The array geometry is shown in Fig. 7. Its aperture diameter, $D/\lambda \approx 14$ (λ is the wavelength), is chosen according to the condition that the beam formed with the plane wavefront in a phased array aperture and directed to the furthermost cell of

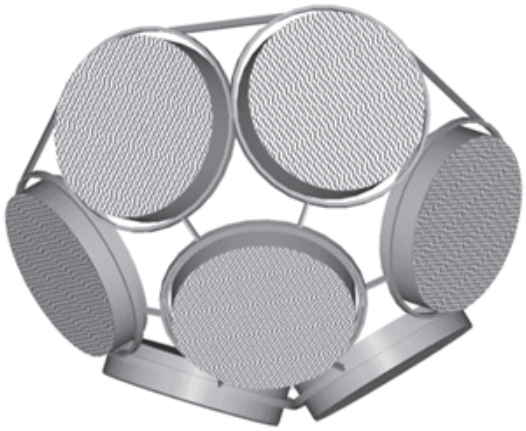

FIGURE 6. Antenna system of seven planar phased arrays with circular apertures.

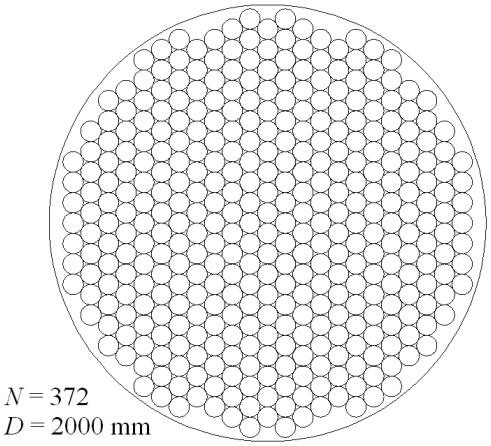

FIGURE 7. Array geometry.

the SA has a level of -4 dB at its corners, which provides the maximum gain in the cell [28]. For the operation frequency $f = 2.17$ GHz, the phased array diameter was chosen to be $D = 2,000$ mm.

The array contains 372 elements located in the nodes of a hexagonal lattice with spacing $d = 93.5$ mm ($d/\lambda = 0.676$). The radiation pattern of the array element was calculated as the pattern of a uniformly excited hexagonal cell occupied by a single array element. Element gain on the operation frequency equals 7.0 dBi (aperture efficiency 100%).

The system SA is the cone with the vertex angle $\theta_{SA} = 75.3°$ with partition into 391 cells, as shown in Fig. 4(a). This cone corresponds to a circle with a diameter of 168 km on the Earth's surface.

The center cell and cells surrounding it in the first two rings occupy the cone with the vertex angle $2\theta_3 \approx 58°$ and are serviced with 19 beams formed by the center phased array of the antenna system. The lateral (slanted) phased arrays form 62 beams each and service 62 cells each, those situated in six sectors that rings 4 to 10 are partitioned into.

It should be noted that for the coverage of this SA with non-shaped beams of the antenna system under consideration, about 1,300 such beams are necessary. In this case, the nadir signal level on the surface will be greater by about 12 dB than at the edge of the SA given the slant range variation.

7. SHAPED BEAM SYNTHESIS

Let us represent the angular dependence of the phased array gain on co-polarization as the product of the element power pattern and squared array factor absolute value, as follows:

$$G(\theta,\varphi) = g_{el} \times |f^{co}(\theta,\varphi)|^2 \times \left| \sum_i a_i e^{j\Phi_i} e^{j\frac{2\pi}{\lambda}(x_i u + y_i v)} \right|^2 \quad (17)$$

where $a_i = |a_i| e^{j\Phi i}$ are complex excitation amplitudes of the array elements; x_i and y_i are coordinates of the elements; g_{el} is the element gain at phased array aperture boresight; $f^{co}(\theta,\varphi)$ is the co-polarized element radiation pattern; and $u = \sin\theta\cos\varphi$ and $v = \sin\theta\sin\varphi$ are the directional cosines of the angles (angles θ and φ are shown in Fig. 1).

Assuming that the array elements are matched and that in their excitation circuits, there are no losses, for the normalized excitation amplitudes, the following relations hold true:

$$|a_i| = \sqrt{p_i/P_0}, \quad P_0 = \sum p_i, \quad \sum |a_i|^2 = 1 \quad (18)$$

where p_i are powers fed to the element inputs of the transmitting array, and P_0 is the total power fed to the elements. The aforementioned assumptions hold true with enough precision for the use in practice in the case of the correct design of the phased array's radiating structure (see, for instance, [29, 30]).

Let us designate the set of the possible array element complex excitation factors (18) meeting the condition of invariant total power fed to the elements with the symbol $\mathbf{A} = \{\mathbf{a} : \Sigma|a_i|^2|\}$.

For shaped radiation pattern synthesis, we use coverage efficiency (CE) as the goal function [19], which is defined as the minimum ratio of the antenna gain (16) to perfect gain (8) within the SA Ω_{SA}:

$$\nu(\mathbf{a}) = \min_{\theta,\varphi\in\Omega_{SA}} \left[\frac{G(\theta,\varphi)}{G_{perf}(\theta,\varphi)} \right] \quad (19)$$

In the case of sidelobe constraints, the goal function must be supplemented with the summand, depending on the maximum gain value in the region Ω_{SL} where sidelobes are to be suppressed:

$$q(\mathbf{a}) = \max_{(\theta,\varphi)\in\Omega_{SL}} G(\theta,\varphi) \quad (20)$$

Let us put down the problem of contoured radiation pattern optimization by the condition of maximum CE in the specified SA with sidelobe constraints as follows, taking into account (19) and (20):

$$w_1 \cdot \nu(\mathbf{a}) - w_2 \cdot q(\mathbf{a}) \to \max_{\mathbf{a}\in\mathbf{A}} \quad (21)$$

where w_1 and w_2 are weights defining the importance of the respective summand.

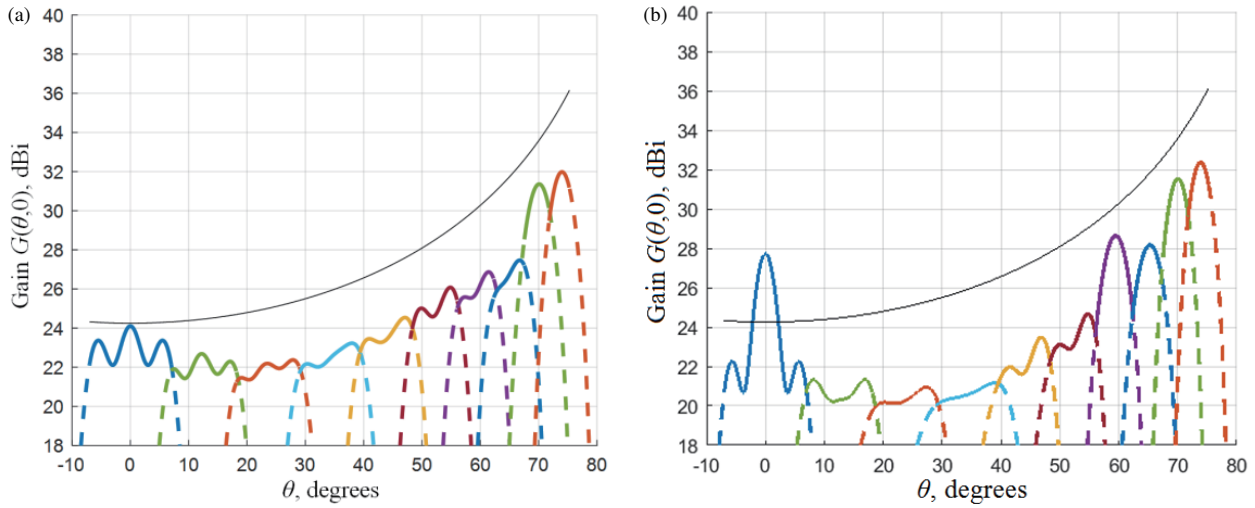

FIGURE 8. Angular dependence of the gain of antenna system shaped beams in the OB section (Fig. 4(a)): (a) amplitude-and-phase synthesis; (b) phase-only synthesis.

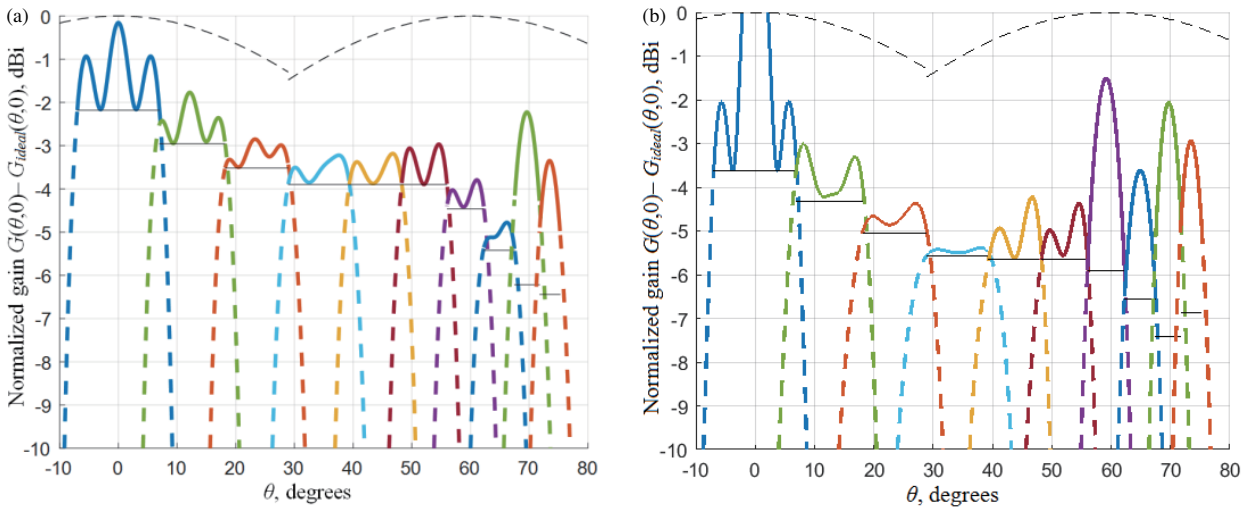

FIGURE 9. Angular dependence of the gain of antenna system shaped beams in the OB section (Fig. 4(a)), normalized to the perfect gain: (a) amplitude-and-phase synthesis; (b) phase-only synthesis.

In case additional requirements are present — such as the maximum gain deviation from the perfect value within the SA, the width of the transition zone at the SA border, the cross-polarization level within the SA, etc. — the goal function is supplemented for these requirements to be reflected in it as well.

To solve the synthesis problem (21), the method of gradient optimization has been used. For numerical optimization, the steepest descent method [31] and log-sum exponential smoothing method [32] have been used.

The sections of contoured radiation patterns (17), optimized in accordance with (21) for cells of the SA considered above (section OB in Fig. 4(a)), are presented in Fig. 8. The contoured radiation patterns are normalized to the isotropic RP — i.e., they represent the angular dependence of the gain. The values of the perfect gain (8) are shown with the solid black line.

In Fig. 9, the gain values normalized to the perfect gain (8) are shown. The horizontal lines within each cell show the minimum function values in each cell, representing the CE values (19).

In Figs. 10 and 11, the aperture distribution for the central beam for amplitude-and-phase and phase-only synthesis is shown as an example. Amplitude distribution for phase-only synthesis is uniform.

The greatest CE $\nu \approx -2.2$ dB has been achieved in the center cell (Fig. 9), whose angular size is approximately four times the size of a non-broadened beam for this antenna. The further from the center the cells, the less the CE, which is caused by both decreasing the angular size of cells and the radiation pattern profile of the phased array element (dashed lines in Fig. 9). The CE of the beams servicing the cells of the outer ring amounts to $\nu < -6$ dB because these cells are covered by virtually non-broadened beams of the MBA aperture [31] and also because their shape does not match the shape of the cells: the beam

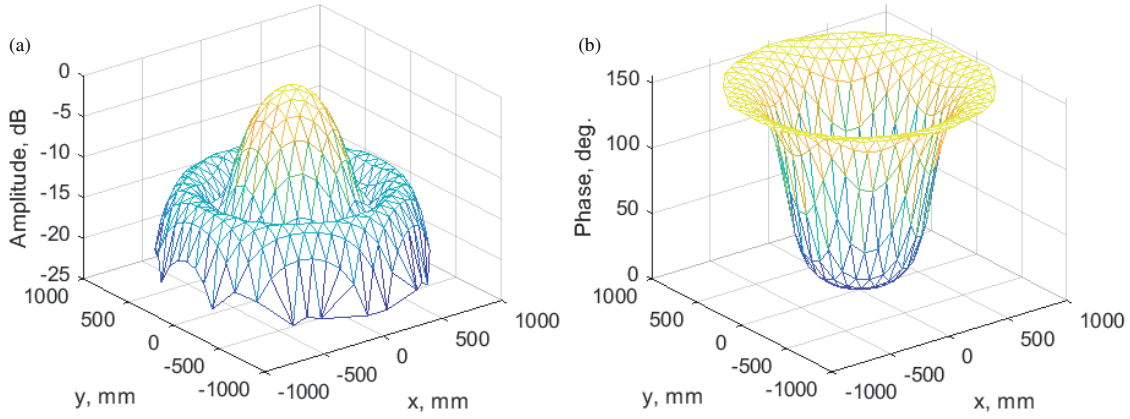

FIGURE 10. Optimized aperture distribution for the central beam, amplitude-and-phase synthesis: (a) amplitude; (b) phase.

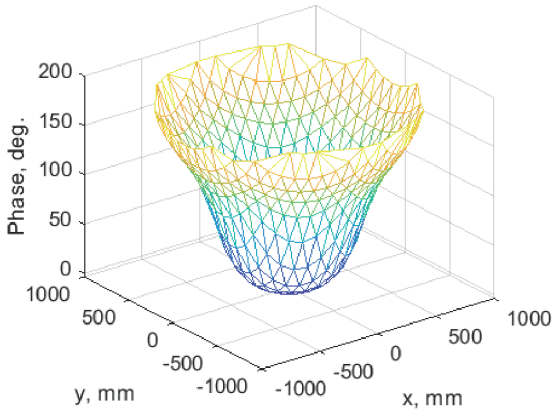

FIGURE 11. Optimized aperture phase distribution for the central beam, phase-only synthesis.

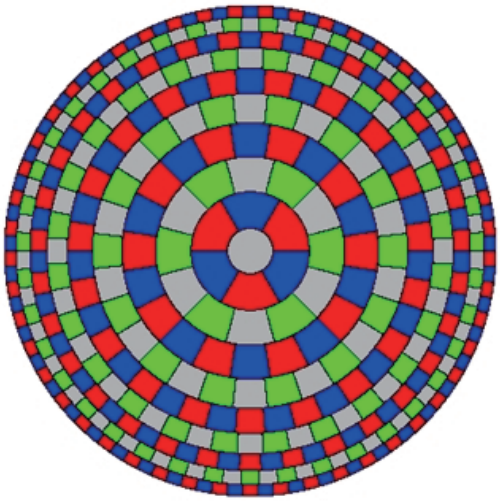

FIGURE 12. Distribution of frequency letters for cells in the case of four letters.

footprints on the plane have an elliptic shape, and the cells have a sector shape.

8. DECOUPLING BETWEEN CONTOURED BEAMS

High throughput of communication systems with MBAs is provided by the spatial and frequency separation of signals in different beams (see, for example, [11, 21, 22, 26, 33]). The neighboring cells are serviced with beams using different frequency letters (sub-bands). For the improvement of decoupling in neighboring cells, orthogonally polarized signals are used as well.

The peaks of beams operating at the same frequency are separated in space. The more frequency letters there are, the further the cells serviced on the same letters can be separated, and the better the spatial decoupling can be achieved.

In Fig. 12, the earlier considered (see Fig. 4(a)) example of an SA is shown, whose cells are serviced using four frequency letters. The frequency letters repeat in cells separated by a single cell.

To increase spatial decoupling, each shaped beam servicing a specified cell must have minimum sidelobes in the cells with other beams at the same frequency.

As an example in Fig. 13, the contoured radiation patterns for servicing the central cell are presented, obtained by the optimization of (21) taking into account (17)–(20). In the first case, only phases of the complex excitation factors of the phased array are optimized (phase synthesis), and in the second case, both amplitudes and phases are optimized (amplitude-and-phase synthesis). In Fig. 14, similar results for a cell in the 3rd ring are shown.

From the presented analysis, it follows that contoured radiation patterns obtained by phase synthesis have sidelobes not exceeding -20 to -25 dB in cells serviced with other beams. The spatial decoupling with those beams amounts respectively to 20–25 dB. However, the signal-to-noise ratio influenced by interference from 95 beams in the cell through their sidelobes amounts only to $C/I \approx 7.5$ dB.

For amplitude-and-phase synthesis, sidelobes in the same cells can be suppressed to the level -30 to -50 dB, which assures a higher value of $C/I = 19$ dB in the system under consideration.

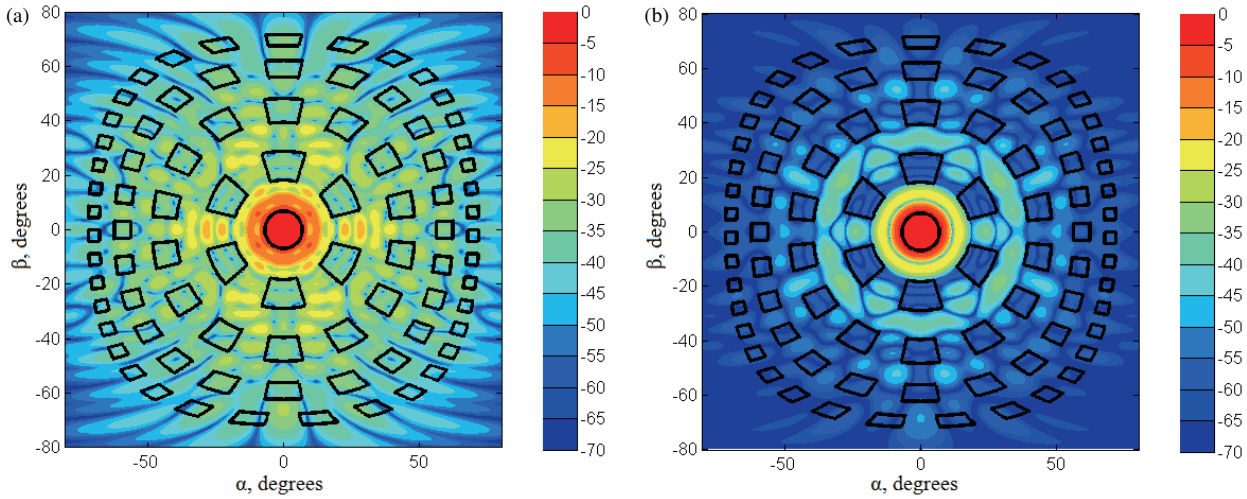

FIGURE 13. Contoured radiation pattern for service of the central cell with sidelobe suppression in cells serviced with other beams in the same frequency sub-band: (a) phase-only synthesis; (b) amplitude-and-phase synthesis. The cells are outlined with solid lines.

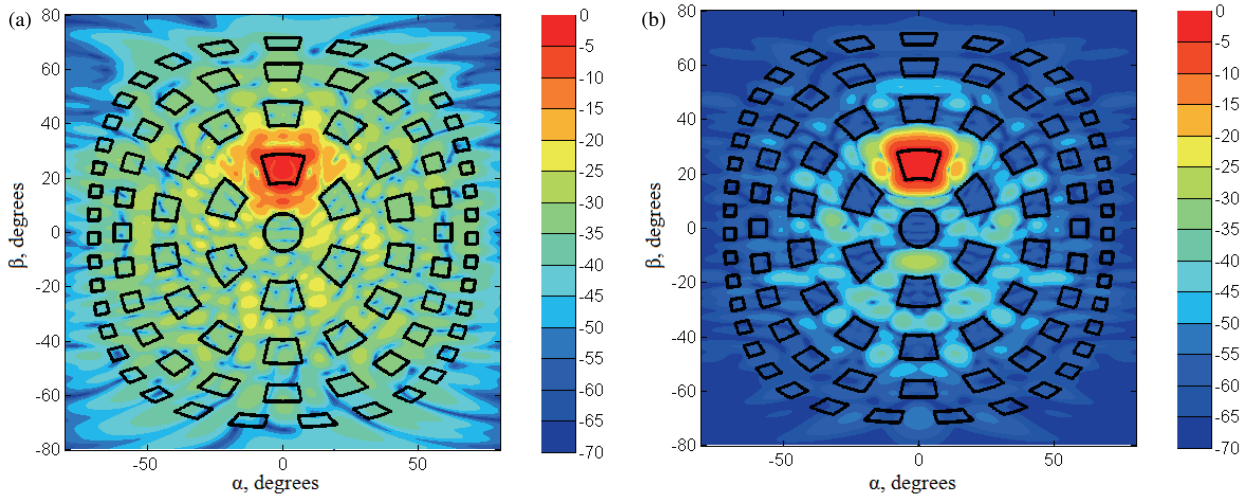

FIGURE 14. Contoured radiation pattern, servicing the cell in the 3rd ring with sidelobe suppression in cells serviced with other beams in the same frequency sub-band: (a) phase-only synthesis; (b) amplitude-and-phase synthesis.

In modern high-throughput communication systems, different digital signals are used [34], whose transmission is possible if C/I is within the range of 10 to 30 dB. In particular, in [35], a value of $C/I = 16.5$ dB is considered as an example.

Thus, the C/I values obtained in this work show the topicality of the problem of MBA optimization to increase the C/I of the beams. Additionally, to increase the information capacity of the communication system, which depends on the number of beams and C/I in them, solving the optimization problem to determine the optimal number of cells in the SA, antenna aperture dimensions, and the number of frequency letters appears topical.

To demonstrate the possibilities of system performance improvement, we limit the SA of the considered antenna to six rings where the angular size of the cells substantially exceeds the in-phase aperture beamwidth, and the antenna forms well-outlined contoured radiation patterns with a CE not lower than -4 dB. In this case, the SA contains $N = 105$ cells and has an angular size $2\theta_{SA} = 111°$ (the SA diameter is about 65 km). In such an SA, each cell experiences interference from no more than 32 beams of the same frequency letter, and the C/I ratio amounts to no less than 15 dB for the phase synthesis of the contoured radiation pattern of the antenna with amplitude distribution in the aperture descending to -10 dB. For amplitude-and-phase synthesis, C/I is not less than 28 dB. Further optimization of the specified parameters is necessary, taking the cross-polarization of the antenna into account.

9. ANTENNA SYSTEM WITH BEAMS OF OPTIMIZED WIDTH

Alongside the multibeam phased array antenna discussed previously, which forms a system of contoured radiation patterns for covering SA cells (Fig. 4(a)), we also consider an MBA

FIGURE 15. MBA represents a system of aperture antennas, the sizes of which are optimized for the coverage of the cells formed with a radial-and-ring grid.

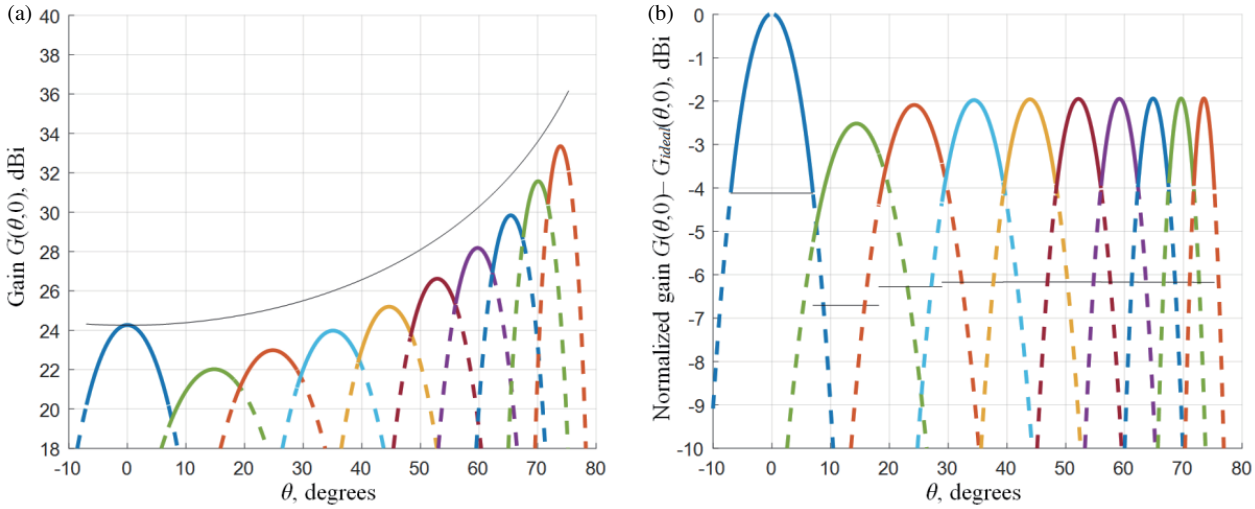

FIGURE 16. Angular dependence of the gains of the antenna system beams in the OB section: (a) normalized to the isotropic radiator; (b) normalized to the perfect gain.

comprising a system of aperture antennas, such as reflectors or horns. Each of these antennas has an axisymmetric aperture with an amplitude distribution descending to zero, forming a single beam. This type of antenna can be used in a V-band repeater for a stratospheric communication system [8, 26]. This approach was also explored in [5]. An example of such an antenna is shown in Fig. 15. The beam of the central antenna is aimed at the nadir, covering the central cell of the SA. The ring tiers of antennas form beams that cover cells in the rings of the SA, as illustrated in Fig. 4(a).

The diameter and orientation of the antennas are optimized to provide the maximum CE (18) in the SA cells. The angular dependencies of the optimized gains of antennas in the OB section (Fig. 4(a)) are shown in Fig. 16. We deem it necessary to draw attention to the fact that of all the presented beams, the central beam has the highest CE value. This is caused by the fact that it has a circular shape matching the beam shape. In the rest of the cells, the CE values are about 2 dB lower because of the mismatch of the round shape of the beam and the sector shape of the cell.

The considered MBA provides the $C/I \approx 14$ dB ratio within the cells. The optimization of the information capacity of the system is possible by optimizing the number of cells and the respective number of aperture antennas, their sizes, and amplitude distributions in the apertures.

A comparison of Figs. 9 and 16 shows that using the antenna with contoured beams makes it possible to increase the CE compared to the axisymmetric beam of optimum width by up to 2–4 dB in the considered beam system. If the aperture of the contoured beam antenna is increased, even higher values of CE can be achieved as well [19]. Higher C/I values can also be achieved in this case.

10. CONCLUSIONS

A method for partitioning a communication system's SA into cells covered by a base station's MBA has been proposed. This method ensures equipotential coverage of the SA by considering the slant range from the station to the subscriber. The approach is based on the concept of the perfect radiation pattern and its perfect gain.

The relations defining the angular sizes of the cells and their total number through the specified gain value in the center of the SA for its partitioning with ring and radial-and-ring grids have been obtained.

An example of the S-band MBA system suspended on a stratospheric dirigible and composed of seven phased array panels with contoured beams has been considered. The contoured radiation patterns of the antenna have been obtained by means of phase-only and amplitude-and-phase synthesis for the SA partitioned into cells with a radial-and-ring grid.

It has been demonstrated that for SA coverage with contoured beams, fewer beams are required than the coverage with non-broadened beams, while maintaining the same minimum gain value in the SA as with non-broadened beams.

The efficiency of cell coverage with the obtained contoured radiation patterns in the central cells is 2–4 dB higher than that when using non-broadened beams. However, this efficiency decreases with increasing distance from the SA center due to the reduction in the angular size of cells.

The possibility of synthesizing contoured radiation patterns that provide a carrier-to-interference ratio within a 105-cell SA of no less than 15 dB for phase-only synthesis and 28 dB for amplitude-and-phase synthesis has been demonstrated. Nevertheless, the correction and optimization of this parameter, considering antenna cross-polarization, are necessary.

The efficiency of cell coverage with a system of single-beam antennas with axisymmetric apertures has been considered. The antenna dimensions and beam orientations were optimized for maximum efficiency. In the considered example, the CE of MBAs with shaped beams is, on average, 2 dB higher than that of antennas with beams of optimized width. Additionally, antennas with shaped beams provide substantially greater beam decoupling.

Further elaboration of this work is possible to determine the optimum size of the antenna aperture, the optimum number of contoured beams, and the frequency letters to maximize the information capacity of the communication system.

ACKNOWLEDGEMENT

The authors thank M. S. Nemirovsky and V. R. Anpilogov for their useful discussions as well as V. I. Melnichuk and D. G. Parinov for their help in antenna simulation.

REFERENCES

[1] Hase, Y., R. Miura, and S. Ohmori, "A novel broadband all-wireless access network using stratospheric platforms," in *VTC '98. 48th IEEE Vehicular Technology Conference. Pathway to Global Wireless Revolution (Cat. No.98CH36151)*, Vol. 2, 1191–1194, Ottawa, ON, Canada, 1998.

[2] Ahn, D.-S., B.-J. Ku, D.-C. Baek, K.-R. Park, and S.-P. Lee, "Conceptual design of the stratospheric communication system in Korea," in *The Second International Symposium on Wireless Personal Multimedia Communications*, 74, 1999.

[3] Karapantazis, S. and F. Pavlidou, "Broadband communications via high-altitude platforms: A survey," *IEEE Communications Surveys & Tutorials*, Vol. 7, No. 1, 2–31, 2005.

[4] Baurreau, F., R. Staraj, F. Ferrero, L. Lizzi, J.-M. Ribero, and J.-P. Chessel, "Stratospheric platform for telecommunication missions," in *2015 IEEE International Symposium on Antennas and Propagation & USNC/URSI National Radio Science Meeting*, 914–915, Vancouver, BC, Canada, 2015.

[5] Thornton, J. and K.-C. Huang, *Modern Lens Antennas For Communications Engineering*, John Wiley & Sons, 2013.

[6] "Minimum performance characteristics and operational conditions for high-altitude platform stations providing IMT-2000 in the bands 1,885–1,980 MHz, 2,010–2,025 MHz," Recommendation ITU-R M.1456, 2000.

[7] ITU-R, "Technical and operational characteristics for the fixed service using high-altitude platform stations in the bands 27.5–28.35 GHz and 31–31.3 GHz," Recommendation ITU-R F.1569, 2002.

[8] ITU-R, "Frequency sharing between systems in the fixed service using high-altitude platform stations and satellite systems in the geostationary orbit in the fixed-satellite service in the bands 47.2–47.5 and 47.9–48.2 GHz," Recommendation ITU-R SF.1481-1, 2000-2002.

[9] Oodo, M., R. Miura, and Y. Hase, "Onboard DBF antenna for stratospheric platform," in *Proceedings 2000 IEEE International Conference on Phased Array Systems and Technology (Cat. No.00TH8510)*, 125–128, Dana Point, CA, USA, 2000.

[10] Park, J.-M., S. A. Ganin, D.-S. Ahn, A. G. Shubov, A. V. Shishlov, A. M. Shitikov, and B.-J. Ku, "Multibeam and multi-faced DBF antenna for HAPS (high altitude platform station)," *Telecommunications Review*, Vol. 12, No. 5, 756–769, 2002.

[11] Nemirovsky, M. S., B. A. Lokshin, and D. A. Aronov, "Essentials of the satellite communication system design," *Moscow, Goryachaya liniya-Telecom*, 432, 2016.

[12] Dietrich, F. J., P. Metzen, and P. Monte, "The Globalstar cellular satellite system," *IEEE Transactions on Antennas and Propagation*, Vol. 46, No. 6, 935–942, 1998.

[13] Lafond, J. C., E. Vourch, F. Delepaux, P. Lepeltier, P. Bosshard, F. Dubos, C. Feat, C. Labourdette, G. Navarre, and J. M. Bassaler, "Thales Alenia Space multiple beam antennas for telecommunication satellites," in *The 8th European Conference on Antennas and Propagation (EuCAP 2014)*, 186–190, The Hague, Netherlands, 2014.

[14] Metzen, P. L., "Globalstar satellite phased array antennas," in *Proceedings 2000 IEEE International Conference on Phased Array Systems and Technology (Cat. No.00TH8510)*, 207–210, Dana Point, CA, USA, 2000.

[15] Rohwer, A. B., D. H. Desrosiers, W. Bach, H. Estavillo, P. Makridakis, and R. Hrusovsky, "Iridium main mission antennas — A phased array success story and mission update," in *2010 IEEE International Symposium on Phased Array Systems and Technology*, 504–511, Waltham, MA, USA, 2010.

[16] Anpilogov, V. R., "Contemporary communication and broadcasting satellites. What kind of satellite Russia needs? Appendix 1: Antennas with contoured radiation pattern," *Technologies and Means of Communication*, No. 6-2, 2005.

[17] Shubov, A. G. and A. V. Shishlov, "Efficiency of shaped-beam antennas," *Electromagnetic Waves and Electronic Systems*, Vol. 2, No. 1, 54–57, 1997.

[18] Shishlov, A. V., "Theory and design of reflector antennas for radio systems with contoured service areas," *Radiotekhnika (Radio Engineering)*, No. 4, 39–49, 2007.

[19] Shishlov, A. V., Y. V. Krivosheev, and V. I. Melnichuk, "Principal features of contour beam phased array antennas," in *2016 IEEE International Symposium on Phased Array Systems and Technology (PAST)*, 1–8, Waltham, MA, USA, 2016.

[20] ITU-R, "Satellite antenna radiation pattern for use as a design objective in the fixed-satellite service employing geostationary satellites," Recommendation ITU-R S.672-4.

[21] Colella, M. J., J. N. Martin, and F. Akyildiz, "The HALO network^{TM}," *IEEE Communications Magazine*, Vol. 38, No. 6, 142–148, 2000.

[22] Fujimoto, K., *Mobile Antenna Systems Handbook*, Artech House, 2008.

[23] Bergmann, J. R., F. J. V. Hasselmann, and M. G. C. Branco, "A shaped reflector antenna for mobile communications," in *IEEE Antennas and Propagation Society International Sympo-*

sium. 1999 Digest. Held in conjunction with: USNC/URSI National Radio Science Meeting (Cat. No.99CH37010), Vol. 3, 2154–2157, Orlando, FL, USA, 1999.

[24] Zang, S. R., J. R. Bergmann, and F. J. S. Moreira, "Omnidirectional dual-reflector antenna with a GO shaped main reflector for an arbitrary far-field pattern in the elevation plane," in *2009 3rd European Conference on Antennas and Propagation*, 3047–3050, Berlin, Germany, 2009.

[25] Ding, Z., "5G: Moving to the next generation in wireless technology," Science Daily, Apr. 2015.

[26] Shishlov, A. V., B. A. Levitan, S. A. Topchiev, V. R. Anpilogov, and V. V. Denisenko, "Multibeam antennas for radar and communication systems," *Journal of Radio Electronics*, No. 7, 1684–1719, 2018.

[27] Kitsuregawa, T., *Advanced Technology in Satellite Communication Antennas: Electrical and Mechanical Design*, Artech House, 1990.

[28] Howell, J. M., "Antenna designer's notebook-maximum off-boresight gain, revisited," *IEEE Antennas and Propagation Magazine*, Vol. 33, No. 2, 49–50, Apr. 1991.

[29] Skobelev, S. P., *Phased Array Antennas with Optimized Element Patterns*, Artech House, 2011.

[30] Indenbom, M. V., "Antenna arrays of mobile surveillance radars. Theory, calculation, designs," *Moscow: Radiotekhnika*, 2015.

[31] Shor, N. Z., *Minimization Methods for Non-differentiable Functions*, Springer Science & Business Media, 2012.

[32] Ben-Tal, A. and M. Teboulle, "A smoothing technique for non-differentiable optimization problems," in *Optimization: Proceedings of the Fifth French-german Conference Held in Castel-novel (varetz), France, Oct. 3-8, 1988*, Vol. 1405, 1–11, 2006.

[33] Anpilogov, V. R., A. V. Shishlov, and A. G. Eydus, "HTS multi-beam antenna systems," *Technologies and Means of Communication*, 54–67, 2013.

[34] ITU-R, "Possibilities for global broadband internet access by fixed-satellite service systems," Recommendation ITU-R S, 2007.

[35] Anpilogov, V. R. and V. Yermilov, "Signal-code constructs in the channels of satellite communications and broadcasting," *Technologies and Means of Communication*, 2011.